Environmental Science and Pollution Research (2019) 26:25596–25608
https://doi.org/10.1007/s11356-019-05813-8

RESEARCH ARTICLE

Nitrogen isotope composition of ammonium in $PM_{2.5}$ in the Xiamen, China: impact of non-agricultural ammonia

Shui-Ping Wu[1,2] · Heng Zhu[1] · Zhe Liu[1] · Lu-Hong Dai[1] · Ning Zhang[1] · James J. Schwab[3] · Chung-Shin Yuan[4] · Jin-Pei Yan[5]

Received: 22 March 2019 / Accepted: 20 June 2019 / Published online: 2 July 2019

Abstract

Since NH_3 is a significant precursor to ammonium in $PM_{2.5}$ and contributes significantly to atmospheric nitrogen deposition but largely remains unregulated in China, the insight into the source of NH_3 emissions by the isotopic investigation is important in controlling NH_3 emissions. In this study, atmospheric concentrations of NH_3 and water-soluble ion composition in $PM_{2.5}$ as well as nitrogen isotope ratios in NH_4^+ ($\delta^{15}N\text{-}NH_4^+$) in Xiamen, China, were measured. Results showed that average NH_3 concentration for the five sites in Xiamen was 7.9 μg m^{-3} with distinct higher values in the warm season and lower values in the cold season, and $PM_{2.5}$ concentration for the two sites (urban and suburban) was 59.2 μg m^{-3} with lowest values in summer. In the $PM_{2.5}$, NH_4^+ concentrations were much lower than NH_3 and showed a stronger positive correlation with NO_3^- than that with SO_4^{2-} suggesting the formation of NH_4NO_3 and equilibrium between NH_3 and NH_4^+. Although the concentrations of NH_3 at the urban site were significantly higher than those at the suburban site, no significant spatial difference in NH_4^+ and $\delta^{15}N\text{-}NH_4^+$ was obtained. The distinct heavier $\delta^{15}N\text{-}NH_4^+$ values in summer than in other seasons correlated well with the equilibrium isotopic effects between NH_3 and NH_4^+ which depend on temperature. The initial $\delta^{15}N\text{-}NH_3$ values were in the range of waste treatment (− 25.42‰) and fossil fuel combustion (− 2.5‰) after accounting for the isotope fractionation. The stable isotope mixing model showed that fossil fuel–related NH_3 emissions (fossil fuel combustion and NH_3 slip) contributed more than 70% to aerosol NH_4^+. This finding suggested that the reduction of NH_3 emissions from urban transportation and coal combustion should be a priority in the abatement of $PM_{2.5}$ pollution in Xiamen.

Keywords Ammonia · Ammonium · $PM_{2.5}$ · Stable nitrogen isotope ratio · Non-agricultural source

Responsible editor: Gerhard Lammel

Electronic supplementary material The online version of this article (https://doi.org/10.1007/s11356-019-05813-8) contains supplementary material, which is available to authorized users.

✉ Shui-Ping Wu
wsp@xmu.edu.cn

[1] Center for Marine Environmental Chemistry and Toxicology, College of Environment and Ecology, Xiamen University, Xiamen 361102, China

[2] Fujian Provincial Key Laboratory for Coastal Ecology and Environmental Studies, Xiamen University, Xiamen 361102, China

[3] Atmospheric Sciences Research Center, University at Albany, SUNY, Albany 12203, USA

[4] Institute of Environmental Engineering, Sun Yat-Sen University, Kaohsiung 80424, China

[5] Key Laboratory of Global Change and Marine-Atmospheric Chemistry, Third Institute of Oceanography, Xiamen 361005, China

Introduction

Ammonia (NH_3) is the most abundant alkaline gas in the atmosphere and can readily react with available sulfuric and nitric acid to generate ammonium sulfate, ammonium bisulfate, or ammonium nitrate which account for a large fraction of the fine particulate matter ($PM_{2.5}$) in many Chinese cities (Huang et al. 2014; Wu et al. 2015; Wang et al. 2015). The enhanced $PM_{2.5}$ has been strongly related to the degradation of visibility, adverse health effects, and climate change. In order to mitigate $PM_{2.5}$ pollution in China, the central government has established strict industrial emission regulations for SO_2 and NO_x (http://datacenter.mep.gov.cn). Nevertheless, recent studies revealed that the lack of NH_3 emissions control could weaken the effectiveness of $PM_{2.5}$ pollution control based simply on SO_2 and NO_x emissions reduction (Wang et al. 2013; Zhang and Wu 2013; Backes et al. 2016; Fu et al. 2017). Our previous studies showed that the emission

densities of NH_3 in the coastal urban areas of Fujian province, China, were significantly higher than those in the inland rural areas due to the non-agricultural NH_3 from highly concentrated population and industries (Wu et al. 2017). In addition, NH_3 is estimated to make a great contribution to the total inorganic nitrogen dry deposition due to its rapid dry deposition velocity with respect to that of fine aerosol NH_4^+ (Russell et al. 2003). The contribution of gaseous NH_3 to inorganic nitrogen deposition in Xiamen Bay, China, was estimated to be 27.4–28.2% which was much higher than that of aerosol NH_4^+ (17.0–17.7%) (Wu et al. 2018). Therefore, the source apportionment of NH_3 would give the policymakers a great help with the future $PM_{2.5}$ pollution control strategies and ecological safety.

It is well established that fertilizer application and livestock waste are the largest contributors of ammonia emissions on a regional scale while non-agricultural ammonia from humans, waste treatment, and fossil fuel–based emissions may be more important in the urban area (Wang et al. 2015, 2018; Chang et al. 2016; Kang et al. 2016; Wu et al. 2017). However, the low temporal-spatial resolution and high uncertainty of the emission inventory could not fulfill the needs of successful mitigation for NH_3. It has been suggested that the stable N isotope ratios ($^{15}N/^{14}N$) of anthropogenic atmospheric N depend in part upon their emission sources (Kundu et al. 2010; Felix et al. 2013; Chang et al. 2016; Pan et al. 2016). Therefore, the stable nitrogen isotope ratio in aerosol ammonium ($\delta^{15}N\text{-}NH_4^+$) have been frequently used to investigate sources and processes of atmospheric ammonia (Yeatman et al. 2001; Kundu et al. 2010; Pan et al. 2016, 2018a, b; Wang et al. 2017; Park et al. 2018). Nevertheless, the $\delta^{15}N\text{-}NH_4^+$ values in aerosols may differ very much from those of the initial emitted $\delta^{15}N\text{-}NH_3$ values due to the kinetic and equilibrium isotope fractionation takes place in the physicochemical process (e.g., adsorption, evaporation) (Heaton et al. 1997; Hayasaka et al. 2004; Kawashima and Kurahashi 2011; Savard et al. 2017). When NH_3 is in deficit, the $\delta^{15}N$ values in NH_4^+ reflect their NH_3 sources (Jickells et al. 2003). In NH_3-rich atmosphere, however, the $^{15}N/^{14}N$ fractionation under equilibrium reaction of gaseous NH_3 to aerosol NH_4^+ should generate higher $\delta^{15}N$ values in NH_4^+ than in NH_3 (Heaton et al. 1997; Savard et al. 2017). An experimental $NH_4^+\text{-}NH_3$ isotopic enrichment factor, $\varepsilon_{NH4^+\text{-}NH3}$ (= $[(^{15}N/^{14}N)_{NH4^+}/(^{15}N/^{14}N)_{NH3} - 1] \times 1000 \approx \delta^{15}N\text{-}NH_4^+ - \delta^{15}N\text{-}NH_3$), was estimated to be + 33‰ (Heaton et al. 1997), which was in fact close to the calculated difference between $\delta^{15}N\text{-}NH_4^+$ and $\delta^{15}N\text{-}NH_3$ (from 19.3 to 48.7‰ with a mean of 30.4 ± 8.2‰) in Niigata Prefecture, Japan (Hayasaki et al. 2004). In addition, the measurements exhibited high mole concentration ratio of gaseous NH_3 to aerosol NH_4^+ (from 1.4 to 22.8 with a mean of 7.5 ± 5.8) confirming that the reaction of gaseous NH_3 to aerosol NH_4^+ was in equilibrium.

Under the equilibrium conditions, both the isotopic enrichment factor and the phase distribution of NH_4^+/NH_3 contribute to the difference between $\delta^{15}N\text{-}NH_4^+$ and $\delta^{15}N\text{-}NH_3$ (Heaton et al. 1997; Li et al. 2012). Assuming that gaseous NH_3 and aerosol NH_4^+ are in the state of a well-mixed closed system and not influenced by primary particulate NH_4^+, the $\delta^{15}N\text{-}NH_3$ values can be estimated by using an isotopic mass balance as follows (Heaton et al. 1997):

$$\delta_{NH3} = \delta_{NH4+} - \varepsilon_{NH4^+\text{-}NH3} \times (1-f) \quad (1)$$

where δ_{NH3} and δ_{NH4+} are the isotope ratios of the initial gaseous NH_3 and final aerosol NH_4^+, respectively, and f is the fraction of the initial NH_3 gas converted to the aerosol NH_4^+. Savard et al. (2017) found that the isotopic difference between $\delta^{15}N\text{-}NH_4^+$ and $\delta^{15}N\text{-}NH_3$ was inversely correlated with the ambient temperature in central and southern Alberta, Canada. Based on the relationship between $NH_4^+{}_{(aq)}\text{-}NH_{3(g)}$ equilibrium constants and temperature from Urey (1947), Pan et al. (2018b) gave a mathematical regression of $\varepsilon_{NH4^+\text{-}NH3}$ as a function of temperature (Kelvin):

$$\varepsilon_{NH4^+\text{-}NH3} = 12.4678 \times 10^3/T - 7.6694 \quad (2)$$

The modeling yielded $\varepsilon_{NH4^+\text{-}NH3}$ of + 34.17‰ at 25 °C which is in fact very close to the measured isotopic enrichment factor of + 33‰ in Heaton et al. (1997). Based on the IsoSource isotopic mixing model (www.epa.gov), Pan et al. (2016, 2018a) calculated the $\delta^{15}N$ value of the initial NH_3 using $\varepsilon_{NH4^+\text{-}NH3}$ of + 33‰ and estimated that up to 90% of NH_3 was from fossil fuel emissions during hazy days in urban Beijing. However, the ambient NH_3 concentrations were simulated from WRF-CMAQ which likely led to the uncertainty of the f value. Similarly, the $\delta^{15}N\text{-}NH_3$ values were calculated using NH_3 concentrations which were not measured during the $PM_{2.5}$ sampling period in Seoul (Park et al. 2018). Chang et al. (2016) measured the $\delta^{15}N$ values of NH_3 collected by Ogawa passive sampler and estimated that the traffic, waste, livestock, and fertilizer contributed 20.4%, 25.9%, 24.0%, and 29.7%, respectively, to ambient NH_3 during the 2014 APEC summit (3–12 November) in Beijing with stringent air quality control measures. Wang et al. (2017) suggested that the equilibrium between NH_3 and NH_4^+ was weak according to the low molecular ratios of NH_3 to $NO_2 + SO_2$ (~ 0.4) and NH_4^+ to ($NO_3^- + SO_4^{2-}$) (~ 1.1) in urban Beijing in January 2013 and the major contributors to total nitrogen in $PM_{2.5}$ were estimated from coal combustion (41%), vehicle exhausts (30%), and domestic waste/sewage (14%) by SIAR (stable isotope analysis in R) model. The selection of major emission sources and atmospheric conditions (NH_3-rich or NH_3-poor) played an important role in the source apportionment of ambient NH_4^+/NH_3 (Heaton et al. 1997; Li et al. 2012).

It has been proved that NH_3 generated from the septic tanks and evaporated from the urban green space might influence the ambient NH_3 to a great extent in the urban area in China

(Chang et al. 2015; Teng et al. 2017). In order to meet the emission standards for nitrogen oxides (NO_x) from heavy-duty diesel trucks in China, AdBlue (pure urea solution) was widely used in SCR (selective catalytic reduction)-equipped engines to convert NO_x into harmless N_2 in the exhaust stream. At some conditions, over-stoichiometric ammonia availability could result in NH_3 slip in a similar way to that from power plant using SCR denitration technology (Pan et al. 2016). In addition, gasoline and liquid petroleum gasoline engines equipped with a three-way catalytic converter (TWC) can produce NH_3 as a byproduct (Livingston et al. 2009; Behera et al. 2013). Furthermore, the use of TWC with low-sulfur gasoline has been proven to increase NH_3 emissions (Mejía-Centeno et al. 2007). Thus, NH_3 emissions from vehicles in China are expected to increase due to the rapid increase of vehicle numbers and the decrease of sulfur content in gasoline and diesel since 2018. Because the ambient NH_3 is subject to the emission sources, weather conditions, and land use types, the establishment of the localized isotopic signatures (δ^{15}N-NH_3) for the major NH_3 emissions sources is a very important step in the process of ambient NH_3/NH_4^+ source apportionment.

Xiamen is a coastal city in southeastern China, beside the Taiwan Strait, with an area of 1700 km^2 and a population of 3.92 million according to the Xiamen Statistic Yearbook of 2017 (http://www.stats-xm.gov.cn/2017/). Besides, the number of tourists and vehicles and the amount of household waste and residential water consumption reached 67.7 million, 1.11 million, 1.74 million tons, and 211.1 million m^3 in 2016, respectively. In the meantime, however, the amount of nitrogen fertilizer and fattening pigs in 2016 dropped 60% and 27% with respect to those in 2007, respectively, due to the urban expansion and population shift from a rural area to an urban area. The present population density in Xiamen Island has surpassed the densities in Hong Kong and Singapore, and there will be an estimated 5.0 million residents by 2020 according to the Xiamen City Urban Master Planning (2010–2020). Based on the emission inventory of NH_3 in Xiamen in 2015, humans (septic tanks and latrines), waste treatment (sewage treatment plant and landfill), and traffic contributed 92.4% of the total emission of NH_3 in Siming district in Xiamen Island, while the emission of NH_3 from fertilizer application and livestock waste contributed 81.3% of the total NH_3 emission in Xiang'an district (Wu et al. 2017). These statistics implied that the contribution of urban non-agricultural sources such as vehicle exhausts, septic tank exhausts, and waste treatment to ambient NH_3 might be highly significant at a local scale in the urban area of Xiamen.

In this study, we conducted a yearlong study of δ^{15}N-NH_4^+ at two sites (urban and suburban) in Xiamen Bay from December 2016 to November 2017 using the fumigation-precipitation method. We also measured ambient NH_3 concentrations from June 2015 to June 2018 at five sites in Xiamen Bay using Ogawa passive samplers, which could be used for the estimation of the initial δ^{15}N-NH_3 values. Several local emission sources were selected to collect NH_3 and aerosol NH_4^+ for stable nitrogen isotope ratio analysis. In the end, we quantified the source contribution to aerosol NH_4^+ based on the IsoSource isotopic mixing model. The results will provide useful information for the mitigation of non-agricultural sources of NH_3 and $PM_{2.5}$ in urban regions in China.

Methods and materials

Ambient $PM_{2.5}$ and NH_3 sampling

$PM_{2.5}$ were sampled at an urban site located in the Siming campus of Xiamen University (SM, 24.45° N, 118.08° E) in the south of Xiamen Island, and a suburban site located in the Xiang'an campus of Xiamen University (XA, 24.62° N,118.23° E) to the northeast of Xiamen Island (Fig. 1). The urban site is situated between two busy roads about 50 m away from the coast and was selected as a typical coastal urban site. The daily traffic flow rate was around 45,800 on weekends and 18,400 on weekdays based on the field observation in October of 2017. The suburban site is surrounded by villages and scattered plots of cropland about 5 km away from the coast. The distance between the two campuses is around 30 km. The traffic volume near the suburban site is much lower than that near the urban site. $PM_{2.5}$ samples were collected for 3 days per month (generally the fifth, fifteenth, and twenty-fifth day) using a high-volume sampler (TH1000C, 1.05 m^3 min^{-1}, Wuhan Tianhong Instruments, Wuhan, China) adapted with a $PM_{2.5}$ impactor. Pall quartz filters (25,000 QAT-UP, Pall Co.) for $PM_{2.5}$ sampling were pre-combusted to 600 °C for 4 h to remove impurities. The sampling was conducted between December 2016 and November 2017. The concentrations of $PM_{2.5}$ (μg m^{-3}) were determined according to the gravimetric difference before and after sampling and the sampling volume. The daily mean concentrations of criteria air pollutants such as SO_2 and NO_2 and meteorological factors including temperature (T), relative humidity (RH), pressure (P), wind speed (WS), wind direction (WD), visibility (Vis), and rainfall (RF) in Xiamen during the sampling periods were obtained from the websites of www.aqistudy.cn and https://rp5.ru, respectively.

Ogawa passive sampler was employed to monitor ambient ammonia concentration at SM, XA, and other three sites (ZZ, IUE, and DD) in the Xiamen Bay from June 2015 to June 2018 (Fig. 1). The Institute of Urban Environment (IUE) is close to two busy expressways, likely influenced by the vehicle exhausts. The Dadeng Middle School (DD) is located in Dadeng Island which is around 1 km to the marine reclamation land at the Xiamen New Airport under construction. The Zhangzhou campus of Xiamen University (ZZ) is

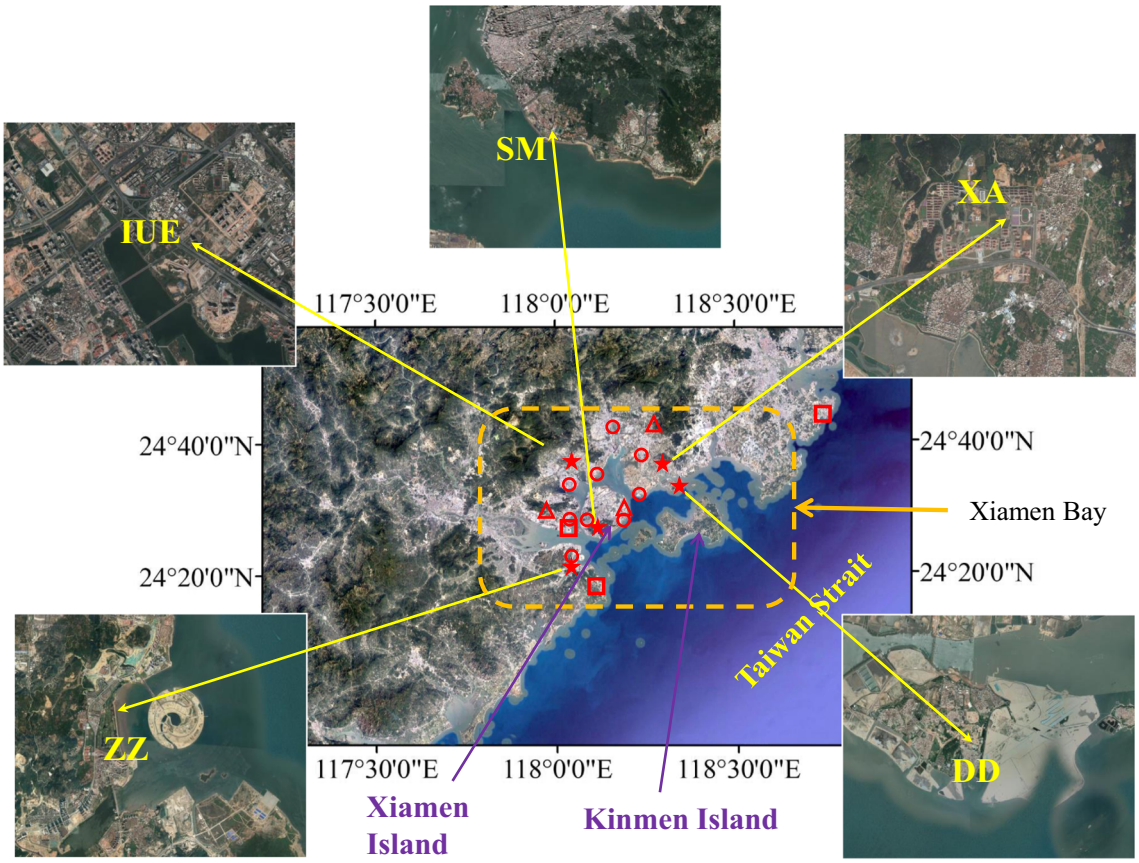

Fig. 1 Location of the $PM_{2.5}$ and NH_3 sampling site (star), power plant (rectangle), waste incineration plant (triangle), and sewage treatment plant (circle) in the Xiamen Bay, China, beside the Taiwan Strait. Approximately 330,000 and 42,000 people live in the inset regions of SM and XA, respectively. SM, XA, and ZZ denote Siming, Xiang'an, and Zhangzhou campuses of Xiamen University, respectively. DD and IUE represent Dadeng Middle School and the Institute of Urban Environment, respectively

located to the south of Xiamen Island around 9 km away from SM. The Ogawa is a double-sided passive diffusion sampler equipped with two 14-mm citric acid-impregnated quartz filters by the manufacturer (www.ogawausa.com). The samplers were deployed for more than 3 weeks per month covering the sampling period of $PM_{2.5}$. The details of sampling sites, surrounding environment, and calculation procedure are available in Wu et al. (2018).

In addition to the ambient NH_3 sampling, for the collection of NH_3 emissions from waste treatment (sewage treatment station, trash transfer station, and public toilet), fertilizer application (urea and organic fertilizers), and biomass burning (rice straw), we used a two-stage filter pack system to sequentially trap particulate NH_4^+ on a PTFE filter (2.0-μm pore size, 30-mm diameter) and gaseous NH_3 on a citrated cellulose filter (2-μm pore size, 30-mm diameter) at a flow rate of 10 L/min. To minimize the interference of ambient atmospheric NH_3/NH_4^+ and isotope fractionation during the sampling period, the evaporated NH_3 was trapped in a semi-closed chamber (0.4 × 0.4 m × 1.0 m) with a hole on the roof for setting sampling inlet. The amount of nitrogen applied for urea and organic fertilizers volatilization experiments was around 100 kg N hm^{-2}, and the volatilized NH_3 was collected on the first, second, and seventh day. For the biomass burning experiment, the smoke particle and gas NH_3 were both sampled for ^{15}N analysis. The confined chamber was first cleaned using a vacuum pump for around 10 min. After waiting for another 10 min until the odors fill the entire chamber, the sampler was turned on to collect NH_3/NH_4^+ for 30 min (Chang et al. 2016).

Chemical and isotope analysis

A punch of quartz filter for $PM_{2.5}$ samples (ϕ 20 mm) and Ogawa NH_3 collection pads were ultrasonically extracted using Milli-Q water (specific resistivity ~ 18.2 MΩ cm). The leachates were analyzed with ion chromatography (PIC-10, Qingdao Puren Instruments Co., China) for NO_3^-, SO_4^{2-}, and NH_4^+ (Wu et al. 2015). The NH_3 concentration was calculated according to the detected amount of NH_4^+ in the collection pad, exposed time (min), average ambient temperature (°C), and concentration conversion coefficient (43.8 ppb min/ng at 20 °C for both pads extracted as one) (https://ogawausa.

com/proctocols/; Wu et al. 2017). A calibration curve was evaluated for each sequence using the standard solutions. A random replicate check was carried out every 10 samples, and the precision fell within 10%. Procedure blanks and recover rates were used to correct the concentrations.

The method for the isolation of ammonium in $PM_{2.5}$ was derived from the HCl fumigation method in Kundu et al. (2010) and Howa et al. (2014). The punch of quartz filter (75-mm diameter) was exposed to HCl fuming in a desiccator overnight to remove NO_3^-. The effectiveness of the approach was evaluated in terms of the remained NH_4^+ and NO_3^- on the filters after HCl fumigation. The extracts of the remained NH_4^+ were filtered to a borosilicate test tube. For the gaseous NH_3 samples, the filter was extracted without HCl fumigation. Excess powered sodium tetraphenylborate (the solubility at 25 °C is 470 g/L) was added to the ammonium salt solutions to ensure complete precipitation of the ammonium ions (Howa et al. 2014). The low solubility of ammonium tetraphenylborate in water (the solubility at 25 °C is 9.7 mg/L) means that very little ammonium remains dissolved form. The precipitates were filtered using a GF/F membrane filter (25-mm diameter, Whatman) and then washed with 5 mL Milli-Q water. The precipitates on the filter papers were allowed to dry for 4.5 h at 55 °C in a vacuum desiccator and then placed in a tin cup for elemental analyzer/isotope ratio mass spectrometer (EA/IRMS) (vario EL cube EA + IsoPrime100, Elementar) to determine nitrogen isotope ratio ($^{15}N/^{14}N$). The tin cups were precleaned with acetone to remove organic contaminants prior to use. It should be noted that the preparation method used in this study for isolating the NH_4^+ fraction of the mixture extract solution might not be interfered by organic nitrogen. The tetraphenylborate isolation method was proved to improve the discriminatory power over bulk analysis (Howa et al. 2014). The solid ammonium tetraphenylborate was oxidized in the combustion column packed with copper oxide at 960 °C, and then the derived NO_2 was introduced into the reduction column to reduce to N_2 at 600 °C. The resultant N_2 gas was purified and transferred to IRMS for isotope measurement. The isotopic composition of N was reported in parts per thousand relative to atmospheric N_2 as follows:

$$\delta^{15}\mathrm{N}\ (‰) = \left[\left(^{15}\mathrm{N}/^{14}\mathrm{N}\right)_{\mathrm{sample}}/\left(^{15}\mathrm{N}/^{14}\mathrm{N}\right)_{\mathrm{N2}}-1\right] \times 1000 \quad (3)$$

where the absolute $^{15}N/^{14}N$ value of N_2 is 3.6765×10^{-3}. A standard with a $\delta^{15}N$ value of 1.18‰ from Indiana University was used as a standard to calculate $\delta^{15}N$ ratios. The average analytical error for $\delta^{15}N$ measurements based on repeated duplicate analysis of the acetanilide standard was 0.25‰.

IsoSource mixing model for source identification

Based on "bottom-up" methods, previous study has indicated that non-agricultural emission sources (humans, waste treatment, and vehicle traffic) contribute around 92% of the total NH_3 emissions in the urban district while agricultural emission sources (fertilizer application and livestock waste) contribute around 81% of the total NH_3 emissions in the suburban district in 2015 (Wu et al. 2017). Considering the surrounding environment at the sampling sites and the prior investigation, the ambient NH_3 near the two sites in Xiamen during the study period have been shown to originate from four major sources: fossil fuel combustion (coal combustion and vehicle exhausts), NH_3 slip (derived from urea that is used in SCR-equipped diesel engines and power plants), N fertilizer application, and human excreta.

The stable nitrogen isotopic composition of a mixture can be used to determine the contribution of different sources using mathematical mixing models. In this study, we used the IsoSource model (version 1.3.1, www.epa.gov) to calculate ranges of source proportional contributions to the initial NH_3. The model solves iteratively for feasible mixing solutions and has been recently used for atmospheric nitrogen source apportionment (Chang et al. 2016; Pan et al. 2016; Wang et al. 2017; Ti et al. 2018). This model addresses every possible combination of source proportions (summing to 100%) incrementally (e.g., 1%), then calculates the predicted isotope value for each combination using linear mass balance equations. These predicted values are then examined to determine which ones fall within some tolerance range (typically 0.1‰) of the observed receptor isotope value, and all of these feasible solutions are recorded.

In this study, the measured $\delta^{15}N\text{-}NH_3$ value from volatilized organic fertilizer (−21.34‰) was used as end member $\delta^{15}N\text{-}NH_3$ value for fertilization because this kind of organic fertilizer was widely used for campus lawn maintenance and vegetables grown near the sampling sites. This value was in the range of reported $\delta^{15}N\text{-}NH_3$ values from rice and wheat field in Taihu lake region, China (Ti et al. 2018), but higher that of the NH_3 volatilization from cornfield in the USA (Felix et al. 2013) and urea in laboratory (Change et al. 2016) (Table S1). Because the sewage treatment plants and trash transfer stations were far away from the two sampling sites, the measured $\delta^{15}N\text{-}NH_3$ values from campus public toilet (−25.42‰) were used as endmember $\delta^{15}N\text{-}NH_3$ value for human excreta. The $\delta^{15}N\text{-}NH_3$ values of NH_3 slip (−12.95‰) were obtained from the measurements in SCR-equipped power plant emissions in Felix et al. (2013) due to the lack of data in China (Pan et al. 2016; Ti et al. 2018). As seen from the Table S1, the $\delta^{15}N\text{-}NH_3$ values in vehicle emissions (−4.6 to −2.2‰ inside tunnel) obtained by Felix et al. (2013) were much heavier than those of −17.8 to −9.6‰ in Chang et al. (2016) but were within the range of coal combustion (−7 to 2‰; Freyer 1978). Thus, the median value of the range of fossil fuel combustion (−2.5‰) from the US-based study was used as the endmember $\delta^{15}N\text{-}NH_3$ value, which can be distinguished from other emissions. The initial $\delta^{15}N\text{-}NH_3$ was

calculated from $\delta^{15}N\text{-}NH_4^+$ according to Eq. (1) because of the isotope exchange equilibrium between NH_3 and NH_4^+ in air (Pan et al. 2016, 2018a).

HYSPLIT backward trajectories

The Hybrid Single-Particle Lagrangian Integrated Trajectory (HYSPLIT) model (https://ready.arl.noaa.gov/) has been widely used to trace the origin of air masses and establish the relationships between source and receptor (Kundu et al. 2010; Beyn et al. 2015). In this study, the backward trajectories were calculated every 6 h with a travel time of 72 h and at 100 m above sea level for each day during the sampling period. Meteorological data were used from the NOAA GDAS (Global Data Assimilation System) database (Su et al. 2015). All the trajectories in each season were separately subjected to cluster analysis using the cluster algorithm of HYSPLIT model. Previous studies have showed that the backward trajectories could be influenced by the starting height (Koracin et al. 2011; Stein et al. 2015). Therefore, the HYSPLIT model was run for starting height at 100 m, 500 m, and 1000 m to investigate the surface influence (Fig. S1). No significant difference was found for the backward trajectory cluster at different starting height. One possible reason for the similar trajectory clusters was that the air mass mainly traveled along the coastal region or from the ocean. The air masses originated from Yangtze River Delta urban agglomerations could carry the coastal urban air pollutants to the sampling sites, while the air masses originated from the South China Sea were clean and could dilute the air pollutants to a great extent.

Results and discussion

Seasonal variation of NH_3 concentration

The annual mean NH_3 concentration for all sites was 7.90 ± 3.79 μg m^{-3} with a range of 1.80 to 22.44 μg m^{-3} ($n = 185$) (Table S2). There were significant positive correlations for the NH_3 concentrations between the five sites ($r = 0.358$–0.691, $p < 0.05$) (Table S3). Generally, the concentrations of NH_3 exhibited higher values in warm season and lower values in cold season (Fig. 2). Significant correlations between NH_3 levels and monthly average site temperature (T) were also observed ($r = 0.345$–0.535, $p < 0.05$, $n = 37$), likely due to the increased NH_3 emissions from soil, fertilization, waste treatment, and green space as well as the dissociation of NH_4NO_3 aerosol brought about by increased temperature (Yeatman et al. 2001; Phan et al. 2013; Hu et al. 2014). However, NH_3 concentration had no correlation with rainfall (RF) and wind speed (WS). In urban Shanghai, there was a highly significant relationship between hourly average WS and NH_3 concentration (Chang et al. 2016). In addition, there were clear morning and evening peaks of NH_3 levels in urban area which were consistent with morning and evening rush hour and mixing layer variations (Wang et al. 2015, 2016). In this study, the triweekly time resolution might cloud the influence of WS and RF on NH_3 concentrations. Therefore, industrial and traffic emissions which are insensitive to temperature could not be the major factor influencing the seasonal pattern of ambient NH_3. Similar temperature dependent patterns have also been reported in urban Shanghai, Beijing, Zhengzhou and Taihu Lake region, China (Wang et al. 2015, 2018; Xu et al. 2016; Ti et al. 2018), and downtown Toronto, Canada (Hu et al. 2014). Notable decrease of NH_4^+ and NO_3^- in $PM_{2.5}$ was observed in the warm season from June to October in Fig. 3 further supporting the effect of temperature on ambient NH_3. Of the five sites, the IUE had significant higher NH_3 concentrations than those at others based on paired-samples t tests ($p < 0.001$, 2-tailed) (Table S4). Because the reclaimed water from the sewage treatment station was applied to the landscape in the office park of IUE, the high levels of NH_3 at this site was probably influenced by NH_3 from both the landscape water body and the vehicular exhausts. Sewage treatment plant has been reported to be an important source of ambient NH_3 in an urban area (Reche et al. 2012; Chang et al. 2016). According to the t test analysis, the ambient NH_3 concentrations at SM were significantly higher than those at XA ($p < 0.001$, 2-tailed) even though N fertilizer application could be an additional emission source at XA. The busy traffic in particular emissions from passenger cars equipped with TWC could make a significant contribution to ambient NH_3 at SM site (Phan et al. 2013; Wang et al. 2016, 2018). Strong positive correlations between NH_3 and CO (mainly emitted as vehicle exhaust) concentrations were observed at the traffic station in Rome (Italy) and a mixed-use urban area (office, commercial, residential, and traffic) east of downtown Shanghai (China) (Perrino et al. 2002; Chang et al. 2016). Similar significant correlations were also observed in urban Seoul in spring, fall, and winter except in summer (Phan et al. 2013). The contribution of vehicle emissions to ambient NH_3 in urban Shanghai was estimated to be 12.6–24.6% based on the difference of the NH_3 concentration above the open section of a traffic tunnel and the ambient concentration at the urban site (Wang et al. 2018). In addition, approximately 330,000 and 42,000 people live in the region around 2 km to SM and XA sites, respectively. Thus, the emissions of NH_3 from residential building toilets and septic tanks were expected to contribute more to the ambient NH_3 at SM than at XA (Chang et al. 2015). The spatial distribution of NH_3 around Xiamen Bay indicated that the urban area is the potential NH_3 emission region in Xiamen.

Table S2 summarizes the reported ambient NH_3 concentration in different cities in the world. The measurements in this study were lower than those determined in Beijing and Xi'an in China, Taihu lake region in China, Santiago in Chile, Rome

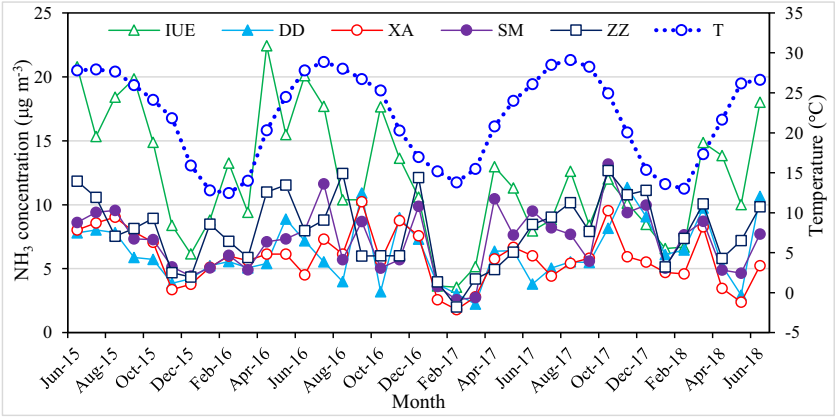

Fig. 2 Monthly variation in NH_3 concentration (IUE, DD, XA, SM, and ZZ) and average temperature (T) in Xiamen Bay, China, from June 2015 to Jun 2018

in Italy, and Okhla and Delhi in India, while higher than those reported in Shanghai and Nanjing in China, Ho Chi Minh City in Vietnam, Madrid in Spain, Niigata in Japan, and some cities in Canada and USA, and were comparable to those measured in urban Seoul (Korea), Barcelona (Spain), and Taichung (China). These comparisons suggested that urban non-agricultural sources could potentially influence ambient NH_3. Generally, the seasonal patterns of NH_3 were characterized by higher values in summer and lower values in winter (Table S2). However, the concentrations of NH_3 in Delhi urban-agro area in India was lower in summer than those in winter and fall due to less agricultural activities in summer (Sharma et al. 2010). Higher ambient NH_3 concentrations were also reported over the cornfield when the fertilizer application rate increased from 40 to 135 kg N ha^{-1} (Felix et al. 2014).

Seasonality of $PM_{2.5}$ and its water-soluble ions

Table 1 summarizes the statistics of $PM_{2.5}$ and its water-soluble ion concentrations. The concentration for $PM_{2.5}$ at SM ranged from 14.0 to 154.8 μg m^{-3} with a mean of 61.8 ± 34.9 μg m^{-3}, which was slightly higher than that at XA (ranged from 13.6 to 123.8 μg m^{-3} with a mean of 56.4 ± 30.9 μg m^{-3}). The $PM_{2.5}$ values in this study were lower than the Chinese National Ambient Air Quality Standard of 75 μg m^{-3} for $PM_{2.5}$ (Grade II, GB3095–2012) but much higher than the annual air quality guideline levels of 25 μg m^{-3} for $PM_{2.5}$ recommended by the World Health Organization (WHO 2006). Although the difference for $PM_{2.5}$ concentration between the two sites was not statistically significant based on the paired t test ($p = 0.404$, 2-tailed) (Table S3), the $PM_{2.5}$ concentrations at the two sites were strongly correlated ($r = 0.592$, $p < 0.001$, $n = 36$). In addition, the average $PM_{2.5}$ concentration at the urban site was slightly higher than the mean value of 51.5 μg m^{-3} in 2011/2013 in the urban area of Xiamen (Wu et al. 2015). Seasonal variations in cations (Na^+, NH_4^+, K^+, Mg^{2+}, and Ca^{2+}), anions (Cl^-, NO_3^-, and SO_4^{2-}), and $PM_{2.5}$ are depicted in Fig. 3. In this study, the trend for $PM_{2.5}$ was higher in the winter, spring, and fall, and lower in the summer. The lower summer values for $PM_{2.5}$ were apparently due to clean air masses from the South China Sea and Taiwan Strait (Figs. S1 and S2), lower gaseous precursors, and higher temperature (Fig. S3) unfavorable for the gas-to-aerosol conversion (Seinfeld and Pandis 2006; Wu et al. 2015). In addition, higher rainfall in summer promotes the scavenging of particles by wet deposition. The sum of the total water-soluble inorganic ions correlated well with $PM_{2.5}$ ($r = 0.331$–0.673, $p < 0.05$) and accounted for 33 ± 16% and 35 ± 20% of $PM_{2.5}$ at SM and XA, respectively. The mass fraction of water-soluble ions in $PM_{2.5}$ were lower than

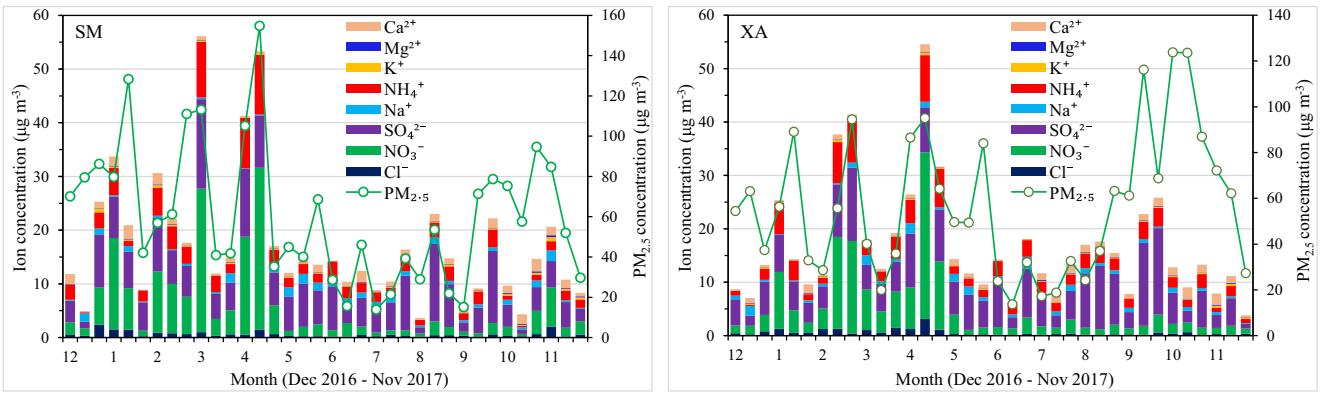

Fig. 3 Variation of $PM_{2.5}$ and its chemical species from December 2016 to November 2017 at SM and XA

Table 1 Mass concentrations of water-soluble ions in $PM_{2.5}$, NH_3, SO_2, NO_2, and molecular ratios of NH_4^+ to NO_3^-, NH_4 to SO_4^{2-}, NH_4^+ to NO_3^- + SO_4^{2-}, NH_3 to NH_4^+, NH_3 to NO_2, NH_3 to SO_2, and NH_3 to NO_2 + SO_2 at SM and XA sites in Xiamen Bay from December 2016 to November 2017

	SM (urban, $n = 36$)		XA (suburban, $n = 36$)	
	Range	Average ± SD	Range	Average ± SD
$sPM_{2.5}$ (μg m^{-3})	14.0–154.8	61.8 ± 34.9	13.6–123.8	56.4 ± 30.9
Na^+ (μg m^{-3})	0.08–1.94	0.54 ± 0.45	0.09–1.33	0.49 ± 0.30
NH_4^+ (μg m^{-3})	0.18–9.49	2.60 ± 2.21	0.22–7.41	2.46 ± 1.80
K^+ (μg m^{-3})	0.03–0.69	0.22 ± 0.14	0.04–0.49	0.18 ± 0.10
Mg^{2+} (μg m^{-3})	0.03–0.40	0.10 ± 0.08	0.04–0.18	0.08 ± 0.03
Ca^{2+} (μg m^{-3})	0.16–3.28	0.68 ± 0.66	0.19–1.16	0.49 ± 0.20
Cl^- (μg m^{-3})	0.01–2.10	0.48 ± 0.48	0.09–2.25	0.44 ± 0.45
NO_3^- (μg m^{-3})	0.51–27.41	5.26 ± 6.91	0.77–28.31	4.31 ± 5.65
SO_4^{2-} (μg m^{-3})	1.06–15.13	6.34 ± 3.30	1.32–14.70	6.30 ± 3.37
SO_2 (μg m^{-3})	7.58–16.94	11.64 ± 4.01	7.81–19.09	12.92 ± 4.10
NO_2 (μg m^{-3})	18.43–49.89	30.94 ± 12.39	22.20–42.27	31.72 ± 7.15
NH_3 (μg m^{-3})	2.57–13.18	7.54 ± 3.31	1.80–9.53	5.36 ± 2.20
n-NH_4^+/n-NO_3^-	0.43–13.46	3.83 ± 3.24	0.57–9.59	3.42 ± 2.14
n-NH_4^+/n-SO_4^{2-}	0.75–6.12	2.29 ± 1.20	0.73–5.50	2.41 ± 1.24
n-NH_4^+/n-(NO_3^- + SO_4^{2-})	0.27–2.49	1.16 ± 0.52	0.32–2.21	1.18 ± 0.40
n-NH_3/n-NH_4^+	0.58–12.69	3.88 ± 3.29	0.34–7.67	2.94 ± 2.28
n-NH_3/n-NO_2	0.14–1.91	0.80 ± 0.49	0.12–1.16	0.49 ± 0.27
n-NH_3/n-SO_2	0.63–6.22	2.78 ± 1.70	0.38–3.41	1.76 ± 0.90
n-NH_3/n-(NO_2 + SO_2)	0.12–1.46	0.61 ± 0.37	0.09–0.87	0.38 ± 0.20

41.1–49.5% in Beijing-Tianjin-Hebei region (Gao et al. 2018), 43% at Qimu Island in Bohai Sea (Zong et al. 2016), and comparable to 35% in urban Guangzhou and 34% in suburban Zhuhai in China (Tao et al. 2017), indicating that the water-soluble inorganic ions might not play a decisive role in ambient $PM_{2.5}$ in Xiamen. Secondary inorganic ions including SO_4^{2-}, NO_3^-, and NH_4^+ (SNA) constituted the majority of the total water-soluble inorganic ions (more than 80%). The proportion was similar to the values in the North China Plain (average 86%) (Xu et al. 2016). It was clear that the increase of $PM_{2.5}$ was associated with the formation of SNA suggesting that the secondary formation of inorganic aerosol played an important role in $PM_{2.5}$ pollution. Furthermore, the NO_3^- concentrations exhibited strong correlation with its precursor NO_2 at SM ($r = 0.81$, $p < 0.001$, $n = 36$) and XA ($r = 0.723$, $p < 0.001$, $n = 36$) while the SO_4^{2-} concentrations correlated with SO_2 only at SM ($r = 0.38$, $p = 0.01$, $n = 36$) and there was no significant correlation between NH_4^+ and NH_3 at both sites (Fig. S4). The NO_3^- in $PM_{2.5}$ is generally in the form of NH_4NO_3 that is formed by the oxidation of NO_x to the gas phase of HNO_3 and then reaction with NH_3. The low temperature in winter and spring can beneficially promote the gas phase of HNO_3 to transform into aerosol NH_4NO_3 (Seinfeld and Pandis 2006).

According to the paired-samples *t* test results for NH_4^+ and NH_3 between SM and XA in Table S4, the spatial difference of NH_4^+ was more influenced by the post-emission atmospheric chemistry than its gaseous precursor in Xiamen. Strong correlations were found between NH_4^+ and SO_4^{2-} and NO_3^- at both sites ($r = 0.59$–0.90, $p < 0.001$, $n = 36$) (Fig. S4). The molecular ratios of NH_4^+ to NO_3^- + SO_4^{2-} and NH_3 to NH_4^+ were on average of 1.16 ± 0.52 and 3.88 ± 3.29 at SM and 1.18 ± 0.40 and 2.94 ± 2.28 at XA, respectively (Table 1). From this point, NH_4^+ was fully neutralized with SO_4^{2-} and NO_3^-, and there might be sufficient equilibrium reactions between gas NH_3 and aerosol NH_4^+ in the atmosphere when gas NH_3 concentration exceeds that of NH_4^+, especially during the warmer season from May to October. In the atmosphere at Maki Monitoring Station in Niigata Prefecture, Japan, the molecular ratios of NH_3 to NH_4^+ ranged from 1.4 to 22.8 with a mean of 7.5 ± 5.8, which were in accordance with the isotopic fractionation under equilibrium conversion of gas NH_3 to aerosol NH_4^+ (Hayasaki et al. 2004). In contrast, the low molar ratios of ambient NH_3 to (NO_2 + SO_2) (< 1) appeared to show ammonia-poor atmospheric conditions during the sampling period at the two sites. Based on the obvious monthly variations of NH_4^+ and NO_3^- concentrations in Fig. 3, it can be assumed that part of NH_4^+ existed as relatively less stable ammonium salts (e.g., NH_4NO_3). It is expected that the diffusion of NH_3 back to the atmosphere during the reversible reaction and equilibrium between NH_3 and NH_4^+ induced significant isotopic fractionation, thus exhibiting much higher δ^{15}N-NH_4^+ values in $PM_{2.5}$ than its initial ammonia sources (Table S1) (Kawashima and Kurahashi 2011). Therefore, a net

isotope effect between NH_4^+-NH_3 ($\varepsilon_{NH4^+\text{-}NH3}$) should be added to Eq. (1) to calculate the $\delta^{15}N$ values of initial NH_3 before putting into IsoSource model.

Isotopic signatures of NH_4-N in $PM_{2.5}$

The $\delta^{15}N$-NH_4^+ values in $PM_{2.5}$ over the study period showed a wide variability among the samples (Fig. 4). The $\delta^{15}N$-NH_4^+ ranged from 5.29 to 26.13‰ with a mean of 13.96 ± 4.56‰ at SM site and from 1.52 to 27.03‰ with a mean of 14.34 ± 5.52‰ at XA site (Table S5); however, they were not statistically different ($p = 0.678$) (Table S4). Our measurements were heavier than those reported in urban Beijing by Pan et al. (2016, 2018a, b), Baengnyeong Island in Korea by Park et al. (2018), urban Colorado in the USA by Moore (1977), rural and coastal sites in Ireland and England by Heaton et al. (1997), and Yeatman et al. (2001) in aerosol, and similar to the measurements in Taihu Lake region in China by Ti et al. (2018), urban Seoul in Korea by Park et al. (2018), rural Niigata in Japan by Hayasaka et al. (2004), Jeju Island in Korea by Kundu et al. (2010), rural Yurihonjo in Japan by Kawashima and Kurahashi (2011), and urban and industrial areas in Alberta, Canada (Savard et al. 2017) in aerosol (Table S5). As summarized in Table S1, the $\delta^{15}N$-NH_4^+ from ocean and inside tunnel were in the range of − 8 to − 5‰ (Jiekells et al. 2003) and 29.6 to 40.0‰ (Park et al. 2018), respectively, which were beyond the scope of the measured $\delta^{15}N$-NH_4^+ values in $PM_{2.5}$ at the coastal sites in this study. So the particulate NH_4^+ from the two emission sources was not likely to be important contributors.

Although the different nitrogen isotope analysis techniques might influence the measurements, the significant differences for the $\delta^{15}N$-NH_4^+ values at different locations over the world as summarized in Table S5 were more affected by the emission sources and/or isotopic fractionation. For the different surroundings between the two sites in this study, the comparison results indicated that the post-emission processes (e.g., equilibrium fractionation between gaseous NH_3 and aerosol NH_4^+) might play a more important role than that of NH_3 emission sources in determining $\delta^{15}N$-NH_4^+ values. At both sites, the seasonal trend for $\delta^{15}N$-NH_4^+ was slightly heavier in the summer (16.06 ± 5.09‰ at SM and 18.91 ± 4.58‰ at XA; June to September) than in other seasons. In addition, a significant positive correlation between ambient temperature and $\delta^{15}N$-NH_4^+ values was observed at both sites ($r = 0.33$, $p < 0.05$ at SM; $r = 0.67$, $p < 0.001$ at XA) (Fig. S4). Similar good correlation between $\delta^{15}N$ ratios and ambient temperature was also observed for PM_{10} collected from Chennai, India, during late winter (Pavuluri et al. 2010). The seasonal trends agreed with the theoretical concepts that temperature effects on isotopic fractionation may also affect the $\delta^{15}N$ values of atmospheric reaction products.

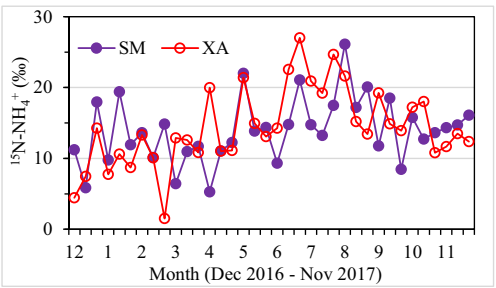

Fig. 4 Variations of $\delta^{15}N$-NH_4^+ (‰) in $PM_{2.5}$ at SM and XA in Xiamen from December 2016 to November 2017

Besides, the seasonality of the $\delta^{15}N$-NH_4^+ values has been often attributed to the changing of the initial $\delta^{15}N$-NH_3 (Kundu et al. 2010; Kawashima and Kurahashi 2011; Park et al. 2018; Ti et al. 2018). Ti et al. (2018) recently reported higher $\delta^{15}N$-NH_3 values from fertilizer application and livestock waste in winter but lower values in summer and fall in Taihu Lake region, China. The peak in spring agricultural activity was accompanied by a decrease in $\delta^{15}N$-NH_3 values at some US ammonia monitoring network sites (Felix et al. 2017). Chang et al. (2016) measured the $\delta^{15}N$-NH_3 values of different volatilized ammonia and found no clear difference between summer and winter. The higher $\delta^{15}N$-NH_4^+ values in summer and fall in Jeju Island and Baengnyeong Island in Korea were more explained by the air mass from China (including enhanced biomass burning) than by isotope fractionation (Kundu et al. 2010; Park et al. 2018). Although the measured $\delta^{15}N$-NH_4^+ values were similar to the $\delta^{15}N$-NH_4^+ values of rice straw burning smoke (Table S1), the average contribution of biomass burning to NH_3 in Xiamen was estimated to be only 0.4% in our previous study (Wu et al. 2017). The facts that the volatilized NH_3 emissions such as animal waste, fertilizer application, and waste treatment with depleted ^{15}N (Table S1) reach maximum due to the highest temperature in summer while the fossil fuel–related NH_3 emissions which are isotopically more enriched in ^{15}N reach maximum in winter due to the energy demand for heating are in conflict with the observed seasonal trend of $\delta^{15}N$-NH_4^+ in this study.

Furthermore, the higher $\delta^{15}N$-NH_4^+ values associated with the stagnant air masses observed in Beijing and Jeju Island (Pan et al. 2018b; Kundu et al. 2010) were consistent with a more pronounced isotope fractionation due to the longer atmospheric lifetime of aerosol NH_4^+ during the transport. It is reasonable to assume that atmospheric chemical reactions caused the lower values of $\delta^{15}N$-NH_4^+ in winter in Korea. In this study, the 3-day backward trajectories from the NOAA's HYSPLIT model in summer appeared to exhibit shorter distance with respect to those in other seasons (Fig. S1) suggesting a possible effect of stagnant air masses on $\delta^{15}N$-NH_4^+ values in summer. In the summer, the high temperature enhances the NH_3 volatilization rates and the NH_3 pool in the atmosphere seems to be filled with NH_3. The enhanced isotope fractionation followed by the intensified gas-to-particle

conversion ($NH_3 \leftrightarrow NH_4^+$) at high NH_3 concentration favors the production of heavier particulate $^{15}NH_4^+$ in the atmosphere (Kawashima and Kurahishi 2011). Therefore, the equilibrium isotope effect between the gaseous NH_3 and aerosol NH_4^+ and its temperature dependence might be the most important factor influencing the seasonality of δ^{15}N-NH_4^+ (Heaton et al. 1997; Kawashima and Kurahashi 2011; Li et al. 2012; Savard et al. 2017).

Contributions of NH_3 to particulate NH_4^+

The initial δ^{15}N-NH_3 values before the start of gas-to-particle conversion were calculated based on the assumption that there existed nitrogen isotope equilibrium exchange between gas NH_3 and aerosol NH_4^+ (Pan et al. 2016; Park et al. 2018). The calculated δ^{15}N-NH_3 values ranged from − 17.48 to − 4.85‰ at SM and from − 20.81 to − 4.11‰ at XA, which were similar to the measured δ^{15}N-NH_3 values of − 11.5 to − 8.5‰ at the highway interchange in urban Seoul (Park et al. 2018), − 14.5 to − 1.0‰ in Niigata Prefecture, Japan (Hayasaki et al. 2004), − 24.2 to −3.0‰ in Taihu Lake region, China (Ti et al. 2018), and − 10 ± 2.6‰ in Colorado, USA (Moore 1977), and were in the range (− 42.4 to +7.1‰) of those reported for 9 AMoN sites across the USA (Felix et al. 2017) but were much higher than those reported in urban Beijing (− 43.1 to − 27.1‰, Chang et al. 2016), near coal-fired power plant (− 38.0 to − 21.1‰) and fertilizer plant (− 31.3‰) in Alberta, Canada (Savard et al. 2017). The calculated δ^{15}N-NH_3 values were generally heavier than those in NH_3 from fertilizer application, livestock excreta, and waste treatment, but lighter than coal combustion and traffic exhausts (Table S1). It should be noted that the measured δ^{15}N-NH_3 values increased from − 32.9‰ on the first day to − 19.06‰ on the second day and − 6.39‰ 7 days after urea application. The trend that volatilized NH_3 after fertilization becomes isotopically heavier over time was also observed in Ti et al. (2018) and Frank et al. (2004). However, the δ^{15}N-NH_3 values changed little for organic fertilizer application experiments. Thus, strong nitrogen fractionation may mask NH_3 source signatures when ambient NH_3 in rural agricultural area is mainly originated from urea fertilizer application.

The IsoSource isotopic mixing model was used to estimate the relative contributions of the four different emission sources on the basis of the calculated δ^{15}N-NH_3 (Fig. 5). The results indicated that fossil fuel combustion—merged with coal combustion and vehicle emissions—dominated the ambient NH_3, with a mean contribution of 44% (in the range of 15–85%) at SM and 59% (in the range of 11–90%) at XA, which were much higher than the results in Taihu Lake region (26%, 19%, and 20% at urban, suburban, and rural sites, respectively) (Ti et al. 2018) and urban Beijing (8.8–29.4%) (Chang et al. 2016). Based on bulk δ^{15}N signatures and a Bayesian isotope mixing model, Wang et al. (2017) estimated

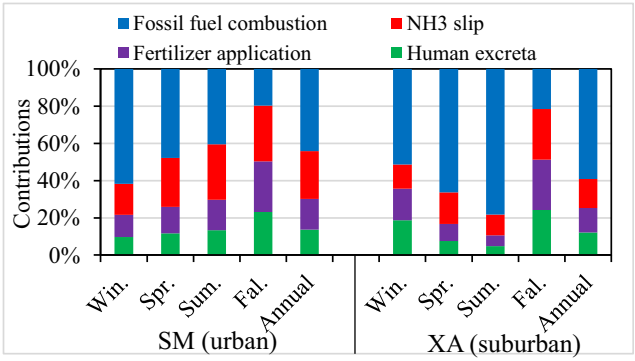

Fig. 5 Relative contributions of individual emissions to atmospheric NH_3 in urban and suburban Xiamen estimated from the IsoSource model

that fossil-derived NH_3 (coal combustion and traffic sources) contributed about 30% of bulk N in $PM_{2.5}$ in urban Beijing. In comparison, fertilizer applications, NH_3 slip, and human excreta only accounted for 13–17%, 16–26%, and 12–14% on average of the ambient NH_3, respectively. The annual contribution ratios of NH_3 from fertilizer application to fossil fuel combustion (0.22–0.37) at the two sites were much lower than the ratio (0.74) at the county level using emission factors (Wu et al. 2017). With a total of 1.11 million civil vehicles in 2016 and a stable growth trend of vehicle numbers and urbanization in Xiamen, regulatory control of urban transportation and coal combustion in Xiamen and surrounding areas will become increasingly important to air quality improvement.

As depicted in previous studies, the uncertainties in the determination for NH_3 end members and isotopic effect taking place during the air-land exchange and gas-aerosol exchange dominate the overall uncertainties in the source apportionment of ambient NH_3 (Chang et al. 2016; Felix et al. 2017; Pan et al. 2018a). As summarized in Table S1, results published for end member data for a single source are variable. In addition, performing near-source sampling to determine site-specific δ^{15}N-NH_3 of individual sources instead of calculating δ^{15}N-NH_3 from δ^{15}N-NH_4^+ values can be made in order to improve and provide statistical confident data (Felix et al. 2017; Savard et al. 2017).

Conclusions

Previous studies have indicated that agricultural emission sources were the largest contributing emission sources to ambient NH_3 at a county or larger scale level, while non-agricultural NH_3 in the urban district could contribute more to the local NH_3 due to its short lifetime. In this study, attempts have been made to measure the ambient NH_3, NH_4^+, and δ^{15}N-NH_4^+ values in $PM_{2.5}$ in Xiamen to separate NH_4^+ into four different source components based on the isotope mixing model. The temperature was identified as the mainspring leading to the seasonal variations of NH_3, NH_4^+, and δ^{15}N-NH_4^+

values. We confirmed that the atmosphere in Xiamen was NH_3-rich based on the high molecular ratios of NH_3 to NH_4^+ and NH_4^+ to NO_3^- + SO_4^{2-} (> 1). A distinct seasonal trend of $\delta^{15}N\text{-}NH_4^+$ values could be detected: lighter in winter and heavier in summer. The initial $\delta^{15}N\text{-}NH_3$ values were calculated under the conditions of nitrogen isotope equilibrium fractionation between gas NH_3 and aerosol NH_4^+. Source apportionment by the IsoSource isotopic mixing model indicated that fossil fuel–related emissions (fossil fuel combustion and NH_3 slip) dominated aerosol NH_4^+ in urban Xiamen, which were basically consistent with the emission inventory in urban Xiamen. These findings suggested that the $\delta^{15}N$ of NH_3 and NH_4^+ can be used as a useful tool to effectively perform source apportionment of atmospheric NH_3 in an urban area and understand how the nitrogen isotope exchange reaction between NH_3 and NH_4^+ is influenced by the temperature. Further studies on the relationship between $\delta^{15}N\text{-}NH_3$ from the emission sources and $\delta^{15}N\text{-}NH_4^+$ at a receptor site can help to develop effective $PM_{2.5}$ control strategies.

Funding information This work was financially supported by the National Key Research and Development Program of China (2016YFC0502901), the Fundamental Research Funds for the Central Universities (No.20720162006), the National Natural Science Foundation of China (No. 41471390), the Natural Science Foundation of Fujian Province of China (No.2017 J01079), and the Key Laboratory of Global Change and Marine-Atmospheric Chemistry, SOA (No. GCMAC1804).

References

Backes AM, Aulinger A, Bieser J, Matthias V, Quante M (2016) Ammonia emissions in Europe, part II: how ammonia emission abatement strategies affect secondary aerosols. Atmos Environ 126:153–161. https://doi.org/10.1016/j.atmosenv.2015.11.039

Behera SN, Sharma M, Aneja VP, Balasubramanian R (2013) Ammonia in the atmosphere: a review on emission sources, atmospheric chemistry and deposition on terrestrial bodies. Environ Sci Pollut Res 20: 8092–8131. https://doi.org/10.1007/s11356-013-2051-9

Beyn F, Matthias V, Aulinger A, Dähnke K (2015) Do N-isotopes in atmospheric nitrate deposition reflect air pollution levels? Atmos Environ 107:281–288. https://doi.org/10.1016/j.atmosenv.2015.02.057

Chang Y, Deng C, Dore AJ, Zhuang G (2015) Human excreta as a stable and important source of atmospheric ammonia in the megacity of Shanghai. PLoS One 10(12):e0144661. https://doi.org/10.1371/journal.pone.0144661

Chang Y, Liu X, Deng C, Dore AJ, Zhuang G (2016) Source apportionment of atmospheric ammonia before, during, and after the 2014 APEC summit in Beijing using stable nitrogen isotope signatures. Atmos Chem Phys 16:11635–11647. https://doi.org/10.5194/acp-16-11635-2016

Felix JD, Elliot EM, Gay DA (2017) Spatial and temporal patterns of nitrogen isotopic composition of ammonia at U.S. ammonia monitoring network sites. Atmos Environ 150:434–442. https://doi.org/10.1016/j.atmosenv.2016.11.039

Felix JD, Elliott EM, Gish TJ, McConnell LL, Shaw SL (2013) Characterizing the isotopic composition of atmospheric ammonia emission sources using passive samplers and a combined oxidation-bacterial denitrifier approach. Rapid Commun Mass Spectrom 27:2239–2246. https://doi.org/10.1002/rcm.6679

Felix JD, Elliott EM, Gish T, Maghirang R, Cambal L, Clougherty J (2014) Examining the transport of ammonia emissions across landscapes using nitrogen isotope ratios. Atmos Environ 95:563–570. https://doi.org/10.1016/j.atmosenv.2014.06.061

Frank DA, Evans RD, Tracy BF (2004) The role of ammonia volatilization in controlling the natural N-15 abundance of a grazed grassland. Biogeochemistry 68(2):169–178. https://doi.org/10.1023/B:BIOG.0000025736.19381.91

Freyer HD (1978) Seasonal trends of NH_4^+ and NO_3^- nitrogen isotope composition in rain collected at Jülich, Germany. Tellus 30:83–92. https://doi.org/10.1111/j.2153-3490.1978.tb00820.x

Fu X, Wang S, Xing J, Zhang X, Wang T, Hao J (2017) Increasing ammonia concentrations recue the effectiveness of particle pollution control achieved via SO2 and NOx emissions reduction in East China. Environ Sci Technol Lett 4:221–227. https://doi.org/10.1021/acs.estlett.7b00143

Gao J, Wang K, Wang Y, Liu S, Zhu C, Hao J, Liu H, Hua S, Tian H (2018) Temporal-spatial characteristics and source apportionment of PM2.5 as well as its associated chemical species in the Beijing-Tianjin-Hebei region of China. Environ Pollut 233:714–724. https://doi.org/10.1016/j.envpol.2017.10.123

Hayasaka H, Fukuzaki N, Kondo S, Ishizuka T, Totsuka T (2004) Nitrogen isotopic ratios of gaseous ammonia and ammonium aerosols in the atmosphere. J Jpn Soc Atmos Environ 39:272–279 https://www.jstage.jst.go.jp/article/taiki1995/39/6/39_6_272/_pdf

Heaton THE, Spiro B, Robertson SMC (1997) Potential canopy influences on the isotopic composition of nitrogen and sulphur in atmospheric deposition. Oecologia 109(4):600–607. https://doi.org/10.1007/s004420050122

Howa JD, Lott MJ, Ehleringer JR (2014) Isolation and stable nitrogen isotope analysis of ammonium ions in ammonium nitrate prills using sodium tetraphenylborate. Rapid Commun Mass Spectrom 28: 1530–1534. https://doi.org/10.1002/rcm.6929

Hu Q, Zhang L, Evans GJ, Yao X (2014) Variability of atmospheric ammonia related to potential emission sources in downtown Toronto, Canada. Atmos Environ 99:365–373. https://doi.org/10.1016/j.atmosenv.2014.10.006

Huang R, Zhang Y, Bozzetti C, Ho K, Cao J, Han Y, Daellenbach KR, Slowik JG, Platt SM, Canonaco F, Zotter P, Wolf R, Pieber SM, Bruns EA, Crippa M, Ciarelli G, Piazzalunga A, Schwikowski M, Abbaszade G, Schnelle-Kreis J, Zimmermann R, An Z, Szidat S, Baltensperger U, Haddad IE, Prévôt ASH (2014) High secondary aerosol contribution to particulate pollution during haze events in China. Nature 514(7521):218–222. https://doi.org/10.1038/nature13774

Jickells TD, Kelly SD, Baker AR, Biswas K, Dennis PF, Spokes LJ, Witt M, Yeatman SG (2003) Isotopic evidence for a marine ammonia source. Geophys Res Lett 30(7):1374. https://doi.org/10.1029/2002GL016728

Kang Y, Liu M, Song Y, Huang X, Yao H, Cai X, Zhang H, Kang L, Liu X, Yan X, He H, Zhang Q, Shao M, Zhu T (2016) High-resolution ammonia emissions inventories in China from 1980 to 2012. Atmos Chem Phys 16:2043–2058. https://doi.org/10.5194/acp-16-2043-2016

Kawashima H, Kurahashi T (2011) Inorganic ion and nitrogen isotopic compositions of atmospheric aerosols at Yurihonjo, Japan: implications for nitrogen sources. Atmos Environ 45:6309–6316. https://doi.org/10.1016/j.atmosenv.2011.08.057

Koracin D, Vellore R, Lowenthal DH, Watson JG, Koracin J, McCord T, DuBois DW, Chen L-WA, Kumar N, Knipping EM, Wheeler NJM, Craig K, Reid S (2011) Regional source identification using Lagrangian stochastic particle dispersion and HYSPLIT backward-

trajectory models. J Air Waste Manage Assoc 61:660–672. https://doi.org/10.3155/1047-3289.61.6.660

Kundu S, Kawamura K, Lee M (2010) Seasonal variation of the concentrations of nitrogenous species and their nitrogen isotopic ratios at Gosan, Jeju Island: implications for atmospheric processing and source changes of aerosols. J Geophysical Res 115:D20305. https://doi.org/10.1029/2009JD013323

Li L, Lollar BS, Li H, Wortmann UG, Lacrampe-Couloume G (2012) Ammonium stability and nitrogen isotope fractionations for NH_4^+-$NH_{3(aq)}$-$NH_{3(gas)}$ systems at 20-70 °C and pH of 2-13: application to habitability and nitrogen cycling in low-temperature hydrothermal systems. Geochim Cosmochim Acta 84:280–296. https://doi.org/10.1016/j.gca.2012.01.040

Livingston C, Rieger P, Winer A (2009) Ammonia emissions from a representative in-use fleet of light and medium-duty vehicles in the California South Coast Air Basin. Atmos Environ 43:3326–3333. https://doi.org/10.1016/j.atmosenv.2009.04.009

Mejía-Centeno I, Martinez-Hernández M, Fuentes GA (2007) Effect of low-sulfur fuels upon NH_3 and N_2O emission during operation of commercial three-ways catalytic converters. Top Catal 42-43:381–385. https://doi.org/10.1007/s11244-007-0210-2

Moore H (1977) Isotopic composition of ammonia, nitrogen dioxide and nitrate in atmosphere. Atmos Environ 11(12):1239–1243. https://doi.org/10.1016/0004-6981(77)90102-0

Pan Y, Tian S, Liu D, Fang Y, Zhu X, Gao M, Gao J, Michalski G, Wang Y (2018b) Isotopic evidence for enhanced fossil fuel sources of aerosol ammonium in the urban atmosphere. Environ Pollut 238:942–947. https://doi.org/10.1016/j.envpol.2018.03.038

Pan Y, Tian S, Liu D, Fang Y, Zhu X, Gao M, Wentworth GR, Michalski G, Huang X, Wang Y (2018a) Source apportionment of aerosol ammonium in ammonia-rich atmosphere: an isotopic study of summer clean and hazy days in urban Beijing. J Geophys Res Atmos 123:5681–5689. https://doi.org/10.1029/2017JD028095

Pan Y, Tian S, Liu D, Fang Y, Zhu X, Zhang Q, Zheng B, Michalski G, Wang Y (2016) Fossil fuel combustion-related emissions dominate atmospheric ammonia sources during severe haze episodes: evidence from ^{15}N-stable isotope in size-resolved aerosol ammonium. Environ Sci Technol 50:8049–8056. https://doi.org/10.1021/acs.est.6b00634

Park YM, Park KS, Kim H, Yu SM, Noh S, Kim MS, Kim YH (2018) Characterizing isotopic compositions of TC-C, NO_3^--N, and NH_4^+-N in $PM_{2.5}$ in South Korea: impact of China's winter heating. Environ Pollut 233:735–744. https://doi.org/10.1016/j.envpol.2017.10.072

Pavuluri CM, Kawamura K, Tachibana E, Swaminathan T (2010) Elevated nitrogen isotope ratios of tropical Indian aerosols from Chennai: implication for the origins of aerosol nitrogen in South and Southeast Asia. Atmos Environ 44:3597–3604. https://doi.org/10.1016/j.atmosenv.2010.05.039

Perrino C, Catrambone M, Di Menno Di Bucchianico A, Allegrini I (2002). Gaseous ammonia in the urban area of Rome, Italy and its relationship with traffic emissions. Atmos Environ 36: 5385–5394. https://doi.org/10.1016/s1352-2310(02)00469-7

Phan N-T, Kim K-Y, Shon Z-H, Jeon E-C, Jung K, Kim N-J (2013) Analysis of ammonia variation in the urban atmosphere. Atmos Environ 65:177–185. https://doi.org/10.1016/j.atmosenv.2012.10.049

Reche C, Viana M, Pandolfi M, Alastuey A, Moreno T, Amato F, Ripoll A, Querol X (2012) Urban NH_3 and sources in a Mediterranean environment. Atmos Environ 57:153–164. https://doi.org/10.1016/j.atmosenv.2012.04.021

Russell KM, Keene WC, Maben JR, Galloway JN, Moody JL (2003) Phase partitioning and dry deposition of atmospheric nitrogen at the mid-Atlantic U.S. coast. J Geophy Res 108(D21):4656. https://doi.org/10.1029/2003JD003736

Savard MM, Cole A, Smirnoff A (2017) Vet R (2017) $\delta^{15}N$ values of atmospheric N species simultaneously collected using sector-based samplers distant from sources – isotopic inheritance and fractionation. Atmos Environ 162:11–22. https://doi.org/10.1016/j.atmosenv.2017.05.010

Seinfeld JH, Pandis SN (2006) Atmospheric chemistry and physics: from air pollution to climate change, second ed. John Wiley and Sons, New Jersey

Sharma SK, Datta A, Saxena TSM, Mandal TK, Ahammed YN, Arya BC (2010) Seasonal variability of ambient NH_3, NO, NO_2 and SO_2 over Delhi. J Environ Sci 22:1023–1028. https://doi.org/10.1016/S1001-0742(09)60213-8

Stein AF, Draxler RR, Rolph GD, Stunder BJB, Cohen MD, Ngan F (2015) NOAA'S HYSPLIT atmospheric transport and dispersion modeling system. Bull Am Meteorol Soc 96:2059–2077. https://doi.org/10.1175/BAMS-D-14-00110.1

Su L, Yuan Z, Fung JCH, Lau AKH (2015) A comparison of HYSPLIT backward trajectories generated from two GDAS datasets. Sci Total Environ 506-507:527–537. https://doi.org/10.1016/j.scitotenv.2014.11.072

Tao J, Zhang L, Cao J, Zhong L, Chen D, Yang Y, Chen D, Chen L, Zhang Z, Wu Y, Xia Y, Ye S, Zhang R (2017) Source apportionment of $PM_{2.5}$ at urban and suburban areas of the Pearl River Delta region, south China – with emphasis on ship emissions. Sci Total Environ 574:1559–1570. https://doi.org/10.1016/j.scitotenv.2016.08.175

Teng X, Hu Q, Zhang L, Qi J, Shi J, Xie H, Gao H, Yao X (2017) Identification of major sources of atmospheric NH_3 in an urban environment in northern China during wintertime. Environ Sci Technol 51:6839–6848. https://doi.org/10.1021/acs.est.7b00328

Ti C, Bao B, Luo Y, Wang X, Wang S, Yan X (2018) Isotopic characterization of NH_x-N in deposition and major emission sources. Biogeochemistry 138:85–102. https://doi.org/10.1007/s10533-018-0432-3

Urey HC (1947) The thermodynamic properties of isotopic substance. J Chem Soc 0: 562–581

Wang R, Ye X, Liu Y, Li H, Yang X, Chen J, Gao W, Yin Z (2018) Characteristics of atmospheric ammonia and its relationship with vehicle emissions in a megacity in China. Atmos Environ 182:97–104. https://doi.org/10.1016/j.atmosenv.2018.03.047

Wang S, Nan J, Shi C, Fu Q, Gao S, Wang D, Cui H, Saiz-Lopez A, Zhou B (2015) Atmospheric ammonia and its impacts on regional air quality over the megacity of Shanghai, China. Sci Rep 5:15842. https://doi.org/10.1038/srep15842

Wang W, Wang S, Xu J, Zhou R, Shi C, Zhou B (2016) Gas-phase ammonia and $PM_{2.5}$ ammonium in a busy traffic area of Nanjing, China. Environ Sci Pollut Res 23:1691–1702. https://doi.org/10.1007/s11356-015-5397-3

Wang Y, Zhang QQ, He K, Zhang Q, Chai L (2013) Sulfate-nitrate-ammonium aerosols over China: response to 2000-2015 emission changes of sulfur dioxide, nitrogen oxides, and ammonia. Atmos Chem Phys 13:2635–2652. https://doi.org/10.5194/acp-13-2635-2013

Wang Y-L, Liu X-Y, Song W, Yang W, Han B, Dou X-Y, Zhao X-D, Song Z-L, Liu C-Q, Bai Z-P (2017) Source appointment of nitrogen in $PM_{2.5}$ based on bulk $\delta^{15}N$ signatures and a Bayesian isotope mixing model. Tellus B 69:1299672. https://doi.org/10.1080/16000889.2017.1299672

WHO (World Health Organization) (2006) Air quality guidelines - global update 2005. World Health Organization Regional Office for Europe, Bonn http://www.euro.who.int/_data/assets/pdf_file/0005/78638/E90038.pdf?ua=1

Wu S-P, Dai L-H, Wei Y, Zhu H, Zhang Y-J, Schwab JJ, Yuan C-S (2018) Atmospheric ammonia measurements along the coastal lines of Southeastern China: implications for inorganic nitrogen deposition to coastal waters. Atmos Environ 177:1–11. https://doi.org/10.1016/j.atmosenv.2017.12.040

Wu S-P, Schwab J, Yang B-Y, Zheng A, Yuan C-S (2015) Two-years $PM_{2.5}$ observations at four urban sites along the coast of southeastern China. Aerosol Air Qual Res 15:1799–1812. https://doi.org/10.4209/aaqr.2015.05.0363

Wu S-P, Zhang Y-J, Schwab JJ, Li Y-F, Liu Y-L, Yuan C-S (2017) High-resolution ammonia emissions inventories in Fujian, China, 2009-2015. Atmos Environ 162:100–114. https://doi.org/10.1016/j.atmosenv.2017.04.027

Xu W, Wu Q, Liu X, Tang A, Dore AJ, Heal MR (2016) Characteristics of ammonia, acid gases, and $PM_{2.5}$ for three typical land-use types in the North China Plain. Environ Sci Pollut Res 23:1158–1172. https://doi.org/10.1007/s11356-015-5648-3

Yeatman SG, Spokes LJ, Dennis PF, Jickells TD (2001) Can the study of nitrogen isotopic composition in size-segregated aerosol nitrate and ammonium be used to investigate atmospheric processing mechanisms? Atmos Environ 35:1337–1345. https://doi.org/10.1016/S1352-2310(00)00457-X

Zhang Y, Wu S-Y (2013) Fine scale modeling of agricultural air quality over the southeastern United States using two air quality models. Part II. Sensitivity studies and policy implications. Aerosol Air Qual Res 13:1475–1491. https://doi.org/10.4209/aaqr.2012.12.0347

Zong Z, Wang X, Tian C, Chen Y, Qu L, Ji L, Zhi G, Li J, Zhang G (2016) Source apportionment of PM2.5 at a regional background site in North China using PMF linked with radiocarbon analysis: insight into the contribution of biomass burning. Atmos Chem Phys 16:11249–11265. https://doi.org/10.5194/acp-16-11249-2016